Influence of various shapes of nanoparticles on unsteady stagnation-point flow of Cu–H_2O nanofluid on a flat surface in a porous medium: A stability analysis

Astick Banerjee[1], Krishnendu Bhattacharyya[2,†], Sanat Kumar Mahato[1], and Ali J. Chamkha[3]

[1] *Department of Mathematics, Sidho-Kanho-Birsha University, Purulia* 723104, *India*
[2] *Department of Mathematics, Institute of Science, Banaras Hindu University, Varanasi* 221005, *India*
[3] *Faculty of Engineering, Kuwait College of Science and Technology, Doha District, Kuwait*

(Received 13 May 2021; revised manuscript received 15 July 2021; accepted manuscript online 1 September 2021)

The nanofluid and porous medium together are able to fulfill the requirement of high cooling rate in many engineering problems. So, here the impact of various shapes of nanoparticles on unsteady stagnation-point flow of Cu–H_2O nanofluid on a flat surface in a porous medium is examined. Moreover, the thermal radiation and viscous dissipation effects are considered. The governing problems of partial differential equations are converted into self-similar coupled ordinary differential equations and those are numerically solved by the shooting method. The computed results can reveal many vital findings of practical importance. Firstly, dual solutions exist for decelerating unsteady flow and for accelerating unsteady and steady flows, the solution is unique. The presence of nanoparticles affects the existence of dual solution in decelerating unsteady flow only when the medium of the flow is a porous medium. But different shapes of nanoparticles are not disturbing the dual solution existence range, though it has a considerable impact on thermal conductivity of the mixture. Different shapes of nanoparticles act differently to enhance the heat transfer characteristics of the base fluid, i.e., the water here. On the other hand, the existence range of dual solutions becomes wider for a larger permeability parameter related to the porous medium. Regarding the cooling rate of the heated surface, it rises with the permeability parameter, shape factor (related to various shapes of Cu-nanoparticles), and radiation parameter. The surface drag force becomes stronger with the permeability parameter. Also, with growing values of nanoparticle volume fraction, the boundary layer thickness (BLT) increases and the thermal BLT becomes thicker with larger values of shape factor. For decelerating unsteady flow, the nanofluid velocity rises with permeability parameter in the case of upper branch solution and an opposite trend for the lower branch is witnessed. The thermal BLT is thicker with radiation parameter. Due to the existence of dual solutions, a linear stability analysis is made and it is concluded that the upper branch and unique solutions are stable solutions.

Keywords: Cu–H_2O nanofluid, various shapes of nanoparticles, unsteady stagnation-point flow, dual solutions, stability analysis

PACS: 47.15.Cb, 47.15.Fe, 44.30.+v **DOI:** 10.1088/1674-1056/ac229b

1. Background of the investigation

The boundary layer flow forms adjacent to the surface on which the fluid flows, so its dynamics and effect are much too important in fluid mechanics. While, the heat transfer in the boundary layer is responsible for cooling the surface and consequently, it is a handy tool for many industries. Now, in this era of science, the ultra-high cooling rate is one of the most crucial requirements of many engineering processes and industries, but the primary limitation is small thermal conductivities of traditional fluids, like, water, oil, ethylene glycol, etc. Previously, solid particles are added in traditional fluids to increase the inherently poor thermal conductivity of those traditional fluids and all efforts are centered on the mixing of micrometer-sized particles, but this approach has some technical shortcomings, such as micro-particles are rapidly deposited as a sediment in fluids, those may block the flow and cause an extra pressure drop. This problem can be settled by adding nanometer-sized particles, called nanoparticles, in aforesaid host fluids and the mixture is known as "nanofluid" proposed by Choi.[1] Adding nanoparticles with typical sizes less than 100 nm in host fluids drastically improves many thermal properties, especially, the thermal conductivities of the mixtures, i.e., nanofluids. To describe the motion of a nanofluid two models have been proposed, namely, "two-phase", and "single-phase" by Buongiorno[2] and Tiwari and Das,[3] respectively. The Tiwari and Das model is more useful between the two for Newtonian base fluids. There are several types of nanoparticles, namely, metals, oxides, carbides, nitrides, or CNTs, which are normally used. Different nanoparticle types have different impacts on the enhancement of thermal conductivity. In addition to the type, the shape of nanoparticles is equally liable to the increase of effective thermal conductivity of the mixture. Maxwell[4] proposed a model for thermal conductivity of a solid-liquid mixture and based on his model the effective thermal conductivity is given by

$$\kappa_{\text{eff, Maxwell}} = \frac{\kappa_{\text{p}} + 2\kappa_{\text{l}} + 2\phi(\kappa_{\text{p}} - \kappa_{\text{l}})}{\kappa_{\text{p}} + 2\kappa_{\text{l}} - \phi(\kappa_{\text{p}} - \kappa_{\text{l}})}\kappa_{\text{l}},$$

†Corresponding author. E-mails: krish.math@yahoo.com; krishmath@bhu.ac.in

where κ_p is thermal conductivity of solid particle and κ_l is thermal conductivity of liquid. Maxwell's model of effective thermal conductivity is based on the assumption that the solid particles are of a spherical shape. Later, Hamilton and Crosser[5] suggested a new model for effective thermal conductivity of the mixture as

$$\kappa_{\text{eff, Ham\&Cros}} = \frac{\kappa_p + (m-1)\kappa_l - (m-1)\phi(\kappa_l - \kappa_p)}{\kappa_p + (m-1)\kappa_l + \phi(\kappa_l - \kappa_p)}\kappa_l,$$

where $m = 3/\psi^*$ represents the shape factor, ψ^* being the sphericity which is defined as the ratio of the surface area of the sphere having same volume to that of the solid particle, to the surface area of the solid particle. So, obviously for spherical-shaped particles m is equal to 3, i.e., for $m = 3$, Hamilton and Crosser's model becomes Maxwell's model. Also, for some standard particle shapes, the values of m are given in Table 1. These two models are independent of size of the solid particles and it means that these two are equally valid for mixtures having nano-sized particles. One can also find some other proposed models[6,7] to describe effective thermal conductivity. Detailed analysis of thermal conductivity of nanofluid with alumina nanoparticles and ethylene glycol base fluid was reported by Beck *et al.*[8] considering various factors along with different shapes of particles. Timofeeva *et al.*[9] experimentally verified the effective thermal conductivity model by Hamilton and Crosser[5] using alumina nanoparticles and the hybrid base fluid consisting of water and ethylene glycol in 1:1 volume ratio. Later, Ellahi *et al.*[10] described the effect of different shapes of nanoparticles on entropy generation in MHD natural convection and Hamid *et al.*[11] discussed the rotating flow of nanofluid along a stretching sheet considering various shapes of MoS_2 nanoparticles. Some other important investigations on nanofluid with various shapes of nanoparticles may be found in the literature.[12–17]

Table 1. The values of shape factor for various shapes of nanoparticles.

Shapes	Spheres	Bricks	Cylinders	Platelets	Blades
m	3	3.7	4.9	5.7	8.6

A porous medium can be used to achieve an adequate cooling rate, i.e., usage of porous media may be treated as a technique for heat transfer enhancement. Porous media are solid materials that have interconnecting pores or voids. So, these are open cell, rigid, and saturated, which indicates that inter-connected pores in the medium are completely filled with some fluid and that fluid may easily flow through the pores. Simultaneous use of both porous media and nanofluid is capable of grabbing substantial attention as new technique to achieve a satisfactory cooling rate with a wide range of applications. For porous media usage, the contact area between fluid and solid surface increases, whereas nanofluids cause enhancement in effective thermal conductivity of the mixture and these increase the rate of heat transfer. The treatment of nanofluids along with porous media has various beneficial applications, such as higher heat transfer, minimum clogging, miniaturization of system, size reduction of heat transfer system, and microchannel cooling, etc. The thermal instability of nanofluid flow in porous medium was investigated by Nield and Kuznetsov[18] taking the Darcy model and Kuznetsov and Nield[19] for the Brinkman model. Ahmad and Pop[20] simultaneously considered nanofluid and porous medium for mixed convection on vertical flat plate, whereas, mixed convection on a vertical wedge was discussed by Gorla *et al.*[21] with similar consideration. Hatami and Ganji[22] took sodium alginate (SA) as a base fluid and titanium dioxide (TiO_2) as nanoparticles to explore heat transfer characteristics for flow inside two coaxial cylinders in a porous medium. Xu *et al.*[23] discussed the forced convective nanofluid flow through foam metals in a duct and reported a pressure drop. Xu and Xing[24] numerically investigated natural convective nanofluids flow in a metal foam cavity using the lattice Boltzmann (LB) model. Convective heat transfer in nanofluid flows in foam metals was studied by Xu *et al.*[25,26] with the local thermal non-equilibrium (LTNE) effect. Later, Xu *et al.*[27] described, in detail, various modes of heat transfer for nanofluid flow in a porous medium. Mehryan *et al.*[28] illustrated the flow of magnetic hybrid nanofluid inside a double-porous medium. Recently, Roşca *et al.*[29] studied stagnation-point flow of nanofluid towards a vertical plate.

Motivated by the engineering requirement of strong cooling rate and by the fact that nanofluid and porous medium together could be able to fulfill the requirement very efficiently, here we investigate the unsteady stagnation-point flow of Cu–H_2O nanofluid on a flat surface in a porous medium taking effect of various shapes of nanoparticles. Viscous dissipation and thermal radiation effects are also considered. This study will explore how the shapes of the nanoparticles play a significant role in controlling heat transfer, i.e., the cooling rate along with other physical parameters. This type of stagnation-point flow problem has many applications, like, the cooling of nuclear reactors and electronic devices, heat exchangers located in a region having small-velocity, solar pond, oil extraction and transportation, photo-catalysis, etc.

2. Problem formulation and basic equations

Consider the unsteady boundary layer flow near a stagnation-point in Cu–H_2O nanofluid over a flat plate embedded in porous medium. The external stagnation-flow velocity is assumed to vary linearly in the form of $u_e(x,t) = ax(1-ct)^{-1}$, where a (> 0) and c are constants. The wall temperature T_w is assumed variable. As y attends to infinity, the value of temperature reaches to a constant value T_∞. In addition, the viscous dissipation effect and thermal radiation are

considered. Under these assumptions, along with the boundary layer structure, the governing equations are

$$\frac{\partial u}{\partial x}+\frac{\partial v}{\partial y}=0, \tag{1}$$

$$\frac{\partial u}{\partial t}+u\frac{\partial u}{\partial x}+v\frac{\partial u}{\partial y}=\frac{\partial u_e}{\partial t}+u_e\frac{\partial u_e}{\partial x}+\upsilon_{nf}\frac{\partial^2 u}{\partial y^2}+\frac{\upsilon_{nf}}{K_1}(u_e-u), \tag{2}$$

$$\frac{\partial T}{\partial t}+u\frac{\partial T}{\partial x}+v\frac{\partial T}{\partial y}=\frac{\kappa_{nf}}{(\rho c_p)_{nf}}\frac{\partial^2 T}{\partial y^2}-\frac{1}{(\rho c_p)_{nf}}\frac{\partial q_r}{\partial y}+\frac{\mu_{nf}}{(\rho c_p)_{nf}}\left(\frac{\partial u}{\partial y}\right)^2. \tag{3}$$

The appropriate boundary conditions are

$$\begin{aligned} &t<0:\ u=0,\ v=0,\ T=T_w \text{ for any } x,\ y,\\ &t\geq 0:\ u=0,\ v=0,\ T=T_w \text{ at } y=0,\\ &u\to u_e(x,t),\ T\to T_\infty \text{ as } y\to\infty, \end{aligned} \tag{4}$$

where u and v are components of velocity along x- and y-axes, respectively, T is temperature of the nanofluid, K_1 $[=K_0/(1-ct)^{-1}]$ is variable permeability of porous material with K_0 being the initial value of permeability, q_r is radiative heat flux, υ_{nf} is kinematic viscosity of the nanofluid, $(\rho c_p)_{nf}$ is heat capacity of the nanofluid, κ_{nf} is thermal conductivity of the nanofluid, μ_{nf} is viscosity of nanofluid, and ρ_{nf} is the density of the nanofluid, which are defined as[30]

$$\rho_{nf}=(1-\phi)\rho_f+\phi\rho_s,\ \ \mu_{nf}=\frac{\mu_f}{(1-\phi)^{2.5}},\ \ \upsilon_{nf}=\frac{\mu_{nf}}{\rho_{nf}},$$

$$(\rho c_p)_{nf}=(1-\phi)(\rho c_p)_f+\phi(\rho c_p)_s,$$

$$\frac{\kappa_{nf}}{\kappa_f}=\frac{\kappa_s+(m-1)\kappa_f-(m-1)\phi(\kappa_f-\kappa_s)}{\kappa_s+(m-1)\kappa_f+\phi(\kappa_f-\kappa_s)}. \tag{5}$$

Here, φ is nanoparticle volume fraction, κ_f and κ_s are thermal conductivities of fluid and of solid nanoparticles, respectively, μ_f is viscosity of base fluid, ρ_f and ρ_s are densities of the fluid and of solid nanoparticles, respectively and m is the shape factor of nanoparticles. The thermophysical properties of considered nanoparticle (Cu) and base fluid (H_2O) are presented in Table 2. Also, various shapes of Cu-nanoparticles are taken into account, namely, sphere-like ($m=3$), brick-like ($m=3.7$), cylinder-like ($m=4.9$), platelet-like ($m=5.7$), and blade-like ($m=8.6$).

The $T_w(x,t)$ is taken in the following form:[31]

$$T_w=T_\infty+T_0\{ax^2/2\upsilon_f\}(1-ct)^{-2}. \tag{6}$$

The radiative heat flux for thermal radiation given by Seddeek and Abdelmeguid[32] is

$$q_r=-\frac{4\sigma}{3k^*_{nf}}\frac{\partial T^4}{\partial y},$$

where σ is a constant called the Stefan–Boltzman constant, k^*_{nf} is the Rosseland absorption coefficient of nanofluid. It is presumed that the variation in temperature within the flow field is such that T^4 may be expanded in a Taylor's series. Expanding T^4 about T_∞ and neglecting higher-order terms we get, $T^4\approx 4T_\infty^3T-3T_\infty^4$.

Table 2. Thermophysical properties of fluid and nanoparticles (Oztop and Abu-Nada[30]).

Physical properties	H_2O	Cu
C_p (J/kgK)	4179	385
ρ (kg/m^3)	997.1	8933
k (W/mK)	0.613	400

Hence, the radiative heat flux may be rewritten as

$$q_r=-\frac{4\sigma}{3k^*_{nf}}\frac{\partial T^4}{\partial y}=-\frac{16\sigma T_\infty^3}{3k^*_{nf}}\frac{\partial^2 T}{\partial y^2} \tag{7}$$

and consequently Eq. (3) reduces to

$$\frac{\partial T}{\partial t}+u\frac{\partial T}{\partial x}+v\frac{\partial T}{\partial y}=\frac{\kappa_{nf}}{(\rho c_p)_{nf}}\frac{\partial^2 T}{\partial y^2}+\frac{16\sigma T_\infty^3}{3k^*_{nf}(\rho c_p)_{nf}}\frac{\partial^2 T}{\partial y^2}+\frac{\mu_{nf}}{(\rho c_p)_{nf}}\left(\frac{\partial u}{\partial y}\right)^2. \tag{8}$$

The following similarity transformations are adopted to do the magic, i.e., to reduce PDEs to ODEs:

$$\eta=\sqrt{\frac{u_e}{\upsilon_f x}}y,\ \ \psi=\sqrt{u_e x\upsilon_f}f(\eta),\ \ \theta(\eta)=\frac{T-T_\infty}{T_w-T_\infty}, \tag{9}$$

where η is the similarity variable, υ_f is the kinematic viscosity of the base fluid and ψ is the stream function defined as $u=\partial\psi/\partial y$ and $v=-\partial\psi/\partial x$, which identically satisfies the equation of continuity (1). In view of relations in Eq. (9), we have the following transformed self-similar ordinary differential equations:

$$\frac{1}{\phi_1}f'''+ff''-f'^2+1+\frac{K}{\phi_1}(1-f')-A\left(f'+\frac{1}{2}\eta f''-1\right)=0, \tag{10}$$

$$\frac{\kappa_{nf}/\kappa_f}{\phi_2}\left(1+\frac{4}{3}R\right)\theta''+Pr\left(f\theta'-2f'\theta\right)-APr\left(2\theta+\frac{1}{2}\eta\theta'\right)+\frac{PrE}{\phi_3}f''^2=0, \tag{11}$$

where $K=\upsilon_f/K_0a$ is the permeability parameter, $A=c/a$ is the unsteady parameter, $Pr=\upsilon_f/[\kappa_f(\rho c_p)_f]$ is the Prandtl number, $R=(4\sigma T_\infty^3)/(\kappa_{nf}k^*_{nf})$ is the radiation parameter, $E=u_e^2/[(c_p)_f(T_w-T_\infty)]$ is the Eckert number and ϕ_1, ϕ_2, ϕ_3 are given as

$$\phi_1=(1-\phi)^{2.5}\left(1-\phi+\phi\frac{\rho_s}{\rho_f}\right),$$

$$\phi_2=\left[1-\phi+\phi\frac{(\rho c_p)_s}{(\rho c_p)_f}\right],$$

$$\phi_3=(1-\phi)^{2.5}\left[1-\phi+\phi\frac{(\rho c_p)_s}{(\rho c_p)_f}\right]. \tag{12}$$

The transformed boundary conditions in (5) are

$$f(0)=0,\quad f'(0)=0,\quad \theta(0)=1,$$
$$f'(\infty)\to 1,\quad \theta(\infty)\to 0. \tag{13}$$

It is well known that the quantities, like skin-friction coefficient $C_{\rm fr}$ (related to surface drag force) and local Nusselt number Nu_x (related to surface heat transfer rate), which are useful and important in physical and engineering viewpoints, are directly proportional to $f''(0)$ and $-\theta'(0)$, respectively and their expressions look like

$$C_{\rm fr}Re_x^{1/2}=\frac{1}{(1-\phi)^{2.5}}f''(0),$$
$$Nu_xRe_x^{-1/2}=-\frac{\kappa_{\rm nf}}{\kappa_{\rm f}}\theta'(0), \tag{14}$$

where $Re_x=u_{\rm e}x/\upsilon_{\rm f}$ is the local Reynolds number.

3. Solution methodology and its validation

The coupled nonlinear Eqs. (10) and (11) with Eq. (12) constitute a BVP and the BVP is numerically solved by a shooting method by converting it into an IVP. We are omitting details of the method,[33–39] which is already available in the literature. To confirm the accuracy of the numerical scheme and computational results, the values of $f''(0)$ for $\phi=0.1$ and $K=0$ are compared with the published results of Bachok *et al.*[40] and Salem *et al.*[41] in Table 3 and the results are found in brilliant agreement. In addition, a graphical comparison of velocity profiles for $A=-0.5$ with $\phi=0$ and $K=0$ with the results of Bachok *et al.*[40] is performed in Fig. 1 and those profiles are observed to have an excellent match.

Table 3. Comparison of the values of $f''(0)$ for different values of A with $\phi=0.1$ and $K=0$.

A	Bachok *et al.*[40]	Salem *et al.*[41]	Present study
1	1.7604	1.7603982	1.760417
−1	1.0845	1.0845304	1.084530
	[−1.1573]	[−1.1572880]	[−1.157300]
−2	0.6499	0.6498771	0.649877
	[−1.9885]	[−1.9885181]	[−1.988516]
−3	0.1045	0.1044666	0.104469
	[−2.3251]	[−2.3251486]	[−2.325146]
−4	−0.6757	−0.67567808	−0.675672
	[−2.2646]	[−2.2646440]	[−2.264642]

[ ] Values for the lower branch solution.

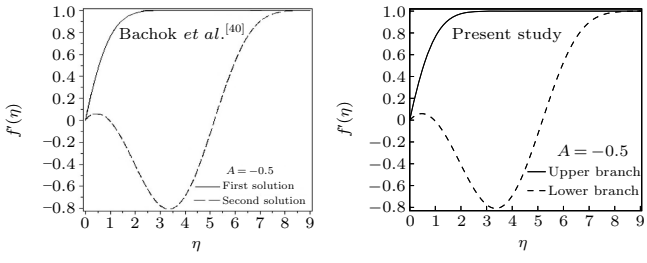

Fig. 1. Comparison of velocity profiles for $A=-0.5$ with $\phi=0$ and $K=0$.

4. Results and discussion

To know the impact of nanoparticles and its various shapes in controlling heat transfer in the unsteady stagnation-point flow of Cu–H_2O nanofluid on a flat surface in a porous medium, the numerically computed results of various physical properties are presented in Figs. 2–18 for different values of involved parameters, namely, the unsteady parameter (A), nanoparticle volume fraction (φ), shape factor of nanoparticles (m), permeability parameter (K), radiation parameter (R), and the Eckert number (E) with the Prandtl number being taken as 6.13 (water) throughout the computations. The volume fraction of nanoparticles is considered 0 and 0.1, where $\varphi=0$ represents the water without any nanoparticle. Results for skin friction coefficient and the Nusselt number demonstrate the existence of dual solutions for any value of decelerating unsteady parameter ($A<0$). But the dual solutions exist up to a certain critical value (say, $A_{\rm c}<0$) of decelerating unsteady parameter and beyond that critical value ($A<A_{\rm c}$) there is no self-similar solution. Whereas, for accelerating unsteady and steady cases ($A\geq 0$), the solution is single, i.e., unique. Due to decelerating unsteadiness of the flow dual solutions exist. The negative value of the unsteady parameter means that the constant c takes a negative value and it is the coefficient of the time variable. It consequently implies that for decelerating unsteadiness, the impact of the time variable on the flow dynamics is completely opposite and it creates a situation of uncertainty as time progresses. Therefore, dual solutions of the flow dynamics are witnessed for decelerating unsteadiness. On the other hand, the presence of nanoparticles only does not affect the critical value, $A_{\rm c}$,[40] but if the medium of flow is a porous medium, then the nanoparticles' presence disturbs the critical value for the existence of dual solutions and so we can accept this as an important finding of the investigation. When the nanoparticle volume fraction is 0.1 then critical value $A_{\rm c}$ is -5.9135 for $K=0.5$ and when $\varphi=0$, $A_{\rm c}$ is -6.4843 for $K=0.5$ (Fig. 2). It directly means that in a porous medium the nanoparticles cause the reduction in the magnitude of $A_{\rm c}$, i.e., the range of existence of dual solutions reduces when nanoparticles are added to the flow field. It is also worth noting that the shapes of nanoparticles have no impact on the aforesaid existence range of dual solutions. In addition, for a unique solution and upper branch solution the drag force enhances due to the presence of nanoparticles for accelerating the unsteady parameter and some cases of decelerating the unsteady parameter. While in the lower branch solution the drag force reduces due to nanoparticles for all values of decelerating the unsteady parameter except near the zero value. Restriction on the surface drag force is very crucial in application viewpoints because the drag force is imposed on the solid surface. In Fig. 3, the Nusselt number is plotted

for different shapes of Cu-nanoparticles, i.e., different values of shape factor m and it is witnessed that as m increases the Nusselt number also increases, i.e., the cooling rate enhances with m. The shape factor is inversely proportional to the sphericity, i.e., the ratio of the surface area of the sphere having equal volume to that of nanoparticle, to the surface area of the nanoparticle. So, as m increases, sphericity decreases, i.e., the surface of the nanoparticle is large and hence the heat-carrying capacity of the nanoparticle becomes higher. As a consequence, the cooling rate is higher when m has larger values. So, the nanoparticles in the form of blades are the best for the heat transfer nanofluid when it is compared with the other shapes (spheres, bricks, cylinders, and platelets) of nanoparticles. Therefore, in many engineering and industrial processes related to heat transfer, blade shape nanoparticles are more beneficial than other shapes considered and so, the shape of nanoparticles can control the heat transfer and hence the final quality of the product. The permeability of the porous medium has a strong influence on the existence range of dual solutions, i.e., on the critical value, A_c (Fig. 4). The range of existence of dual solutions is wider when the permeability parameter is larger. The values of A_c are -4.5066, -5.9135, and -7.4581 for $K = 0$, $K = 0.5$, and $K = 1$. The permeability parameter is inversely proportional to the permeability of porous material. So, as K increases the permeability of porous medium becomes less, i.e., the Darcy resistive force due to porous medium is larger and it results in a significant augmentation of the range of existence of dual solutions. For the same reason, the drag force, i.e., the skin friction coefficient is noticeably high with the permeability parameter in the upper branch solution and unique solution. For different values of K, the Nusselt number is plotted for all considered values of shape factor m, i.e., for various shapes of Cu-nanoparticles in Fig. 5. For the upper branch solution, the Nusselt number, i.e., the cooling rate rises with K for all shapes of considered Cu-nanoparticles and physically, it is the consequence of less permeability of the porous medium. For less a permeable porous medium, i.e., for a more compact porous medium though momentum transport obstructed, but it is quite suitable for high heat transport. So, this very high heat transfer rate due to porous medium in the nanofluid flow has colossal applications in many industrial and engineering problems, like the cooling of electronic devices, the cooling of metallic sheets, etc., while in the lower branch the contrasting effect is witnessed. The impact of the radiation parameter and the Eckert number on the cooling rate, i.e. the Nusselt number, are depicted in Figs. 6 and 7, respectively. The cooling rate is higher for larger values of the radiation parameter. It implies that as the thermal radiation level is high the cooling rate raises and physically this is the excepted outcome. Whereas, a non-zero Eckert number cooling rate slightly reduces for many cases of

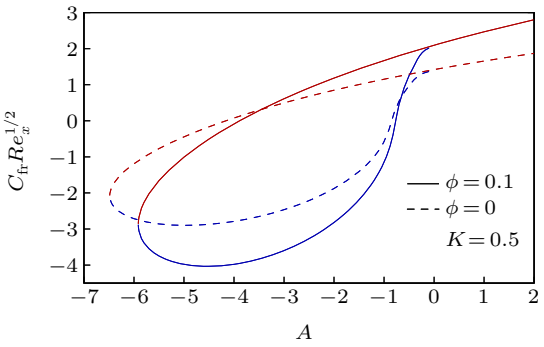

Fig. 2. Skin-friction coefficient, $C_{fr}Re_x^{1/2}$ with A for different nanoparticle volume fractions.

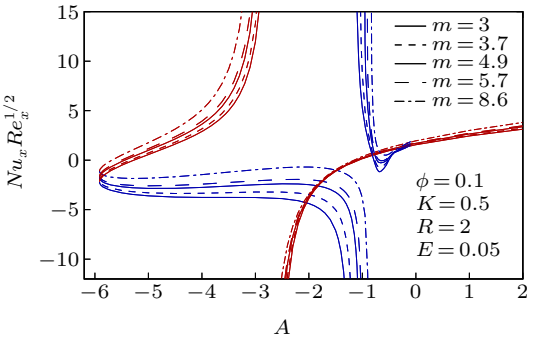

Fig. 3. Nusselt number, $Nu_xRe_x^{-1/2}$ with A for different shapes of nanoparticles.

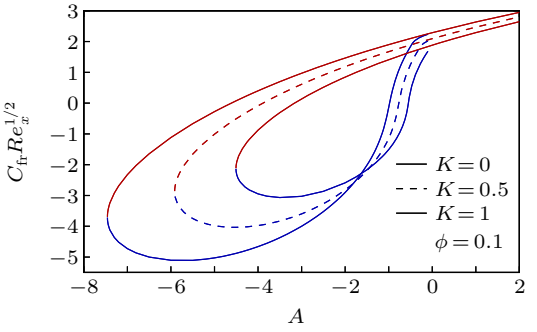

Fig. 4. Skin-friction coefficient, $C_{fr}Re_x^{1/2}$ with A for different values of K.

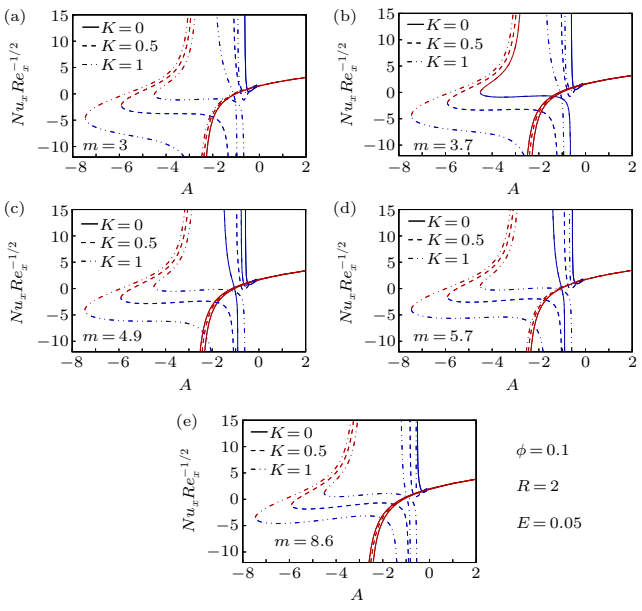

Fig. 5. Nusselt number, $Nu_xRe_x^{-1/2}$ with A for different values of K.

decelerating unsteady flow and for accelerating unsteady flow a minute enhancement in cooling rate is observed. Moreover, in Fig. 8 the Nusselt number is plotted with R for different E and m. It reveals that the effect of the Eckert number on heat transfer coefficient is less prominent with the rise of radiation and the radiation has a considerable impact on heat transfer for different-shaped nanoparticles. Radiative heat transfer is very effective, like convective heat transfer in the presence of nanoparticles.

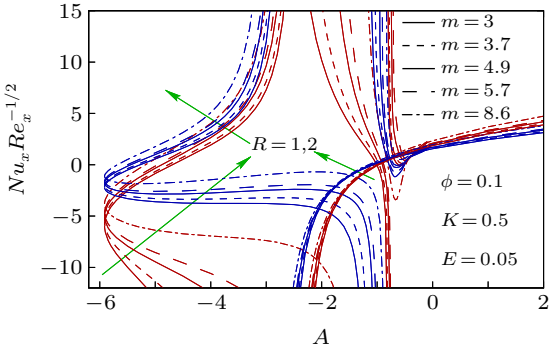

Fig. 6. Nusselt number, $Nu_xRe_x^{-1/2}$ with A for different values of R.

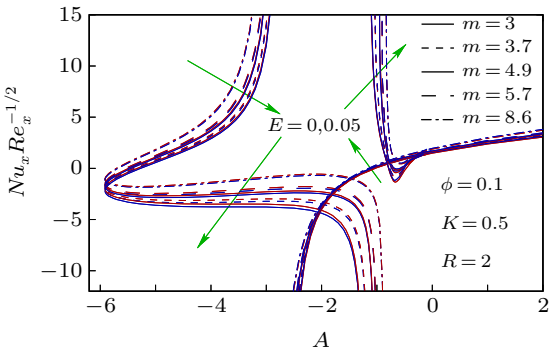

Fig. 7. Nusselt number, $Nu_xRe_x^{-1/2}$ with A for different values of E.

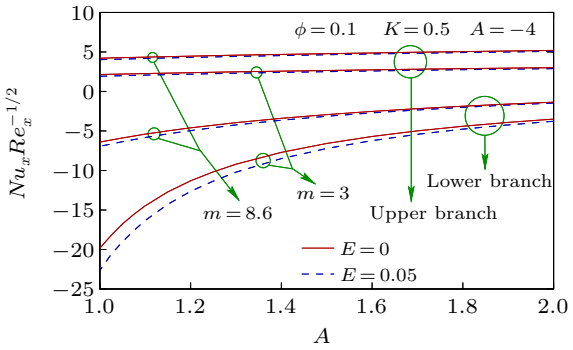

Fig. 8. Nusselt number $Nu_xRe_x^{-1/2}$ with R for different values of E.

For different values of Cu-nanoparticle volume fraction φ, the velocity profiles are shown in Fig. 9. For both solution branches, in spite of initial decay in velocity the boundary layer thickness (BLT) is reduced with φ. Due to the nanoparticle presence the intermolecular force increases and as a consequence, the free stream velocity is achieved earlier and it causes the decline of BLT. In Fig. 10, the temperature profile $\theta(\eta)$ is plotted for all considered values of shape factor m. It exhibits an early decrease of temperature and an increased thermal BLT with m. In reality, the high heat transfer rate with larger m (due to larger surface area) affects free stream temperature up to a longer distance from the flat surface and therefore thermal BLT becomes thick.

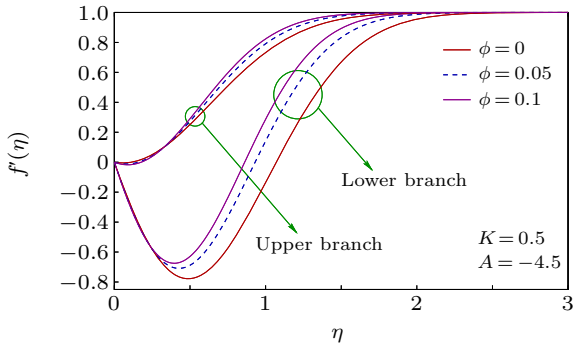

Fig. 9. Velocity profiles for different nanoparticle volume fractions.

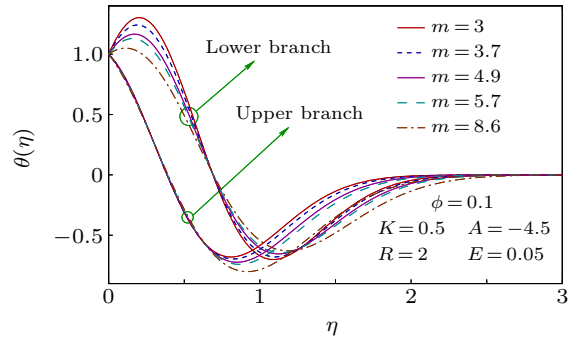

Fig. 10. Temperature profiles for different shapes of nanoparticles.

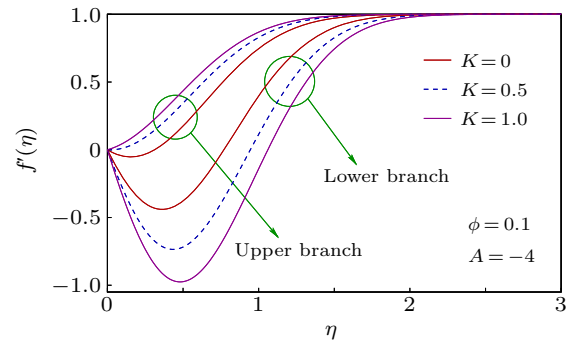

Fig. 11. Velocity profiles for different K.

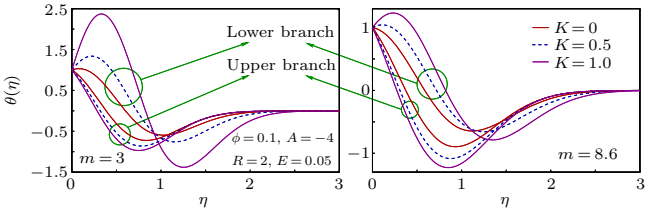

Fig. 12. Temperature profiles for different K.

The impact of permeability parameter K (related to the permeability of the porous medium) on the nanofluid velocity and temperature profiles are illustrated in Figs. 11 and 12. It exhibits contrasting effects on two solution branches. In the

upper branch solution, the velocity rises with K and BLT turns out to be thinner. The Darcy resistive force in porous medium is inversely proportional to its permeability and therefore, with the rise of K, i.e., and with a medium having less permeability, this force grows. Consequently, a shrink of BLT occurs. Whereas the temperature (plotted for two values of m) inside the boundary layer shows a decay with K in the upper branch and lower branch temperature exhibits an initial rise, while away from the surface, the reverse result is found.

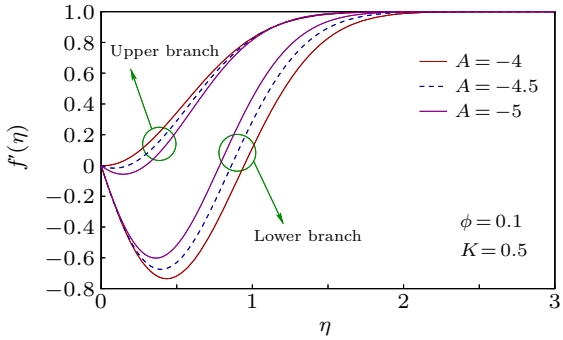

Fig. 13. Velocity profiles for different A (<0, decelerating unsteady flow).

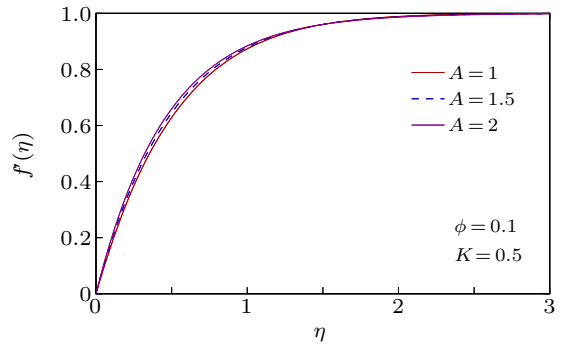

Fig. 14. Velocity profiles for different A (>0, accelerating unsteady flow).

The nanofluid velocity profiles are displayed in Figs. 13 and 14 for decelerating and accelerating unsteady flows. Due to increasing magnitude of decelerating unsteady parameter ($A<0$), the flow velocity reduces in the upper branch solution and it increases with accelerating unsteady parameter ($A>0$). Decelerating unsteadiness of the flow creates such a situation, for which dual solutions exist and no other parameter can control this uncertain situation of the flow. It is already witnessed that the Darcy force of porous medium increases the region of uncertainty of dual solutions. Whereas accelerating unsteadiness is natural and has no ambiguous property, like decelerating unsteadiness and consequently, the solution becomes unique. In Figs. 15 and 16, the nanofluid temperature profiles are presented for various values of A. For decelerating unsteady flow, the temperature rises with increasing magnitude of A in the upper branch with thermal BLT being thinner and though the initial behavior is the opposite for the lower branch, thermal BLT reduces with a magnitude of A. Whereas the nanofluid temperature decreases with A in unique solution for accelerating unsteady flow.

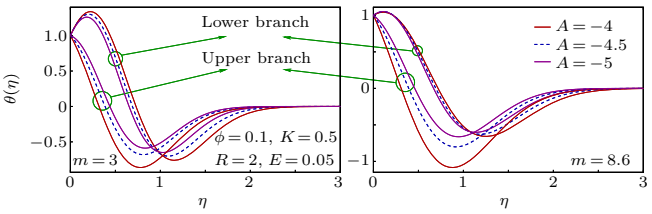

Fig. 15. Temperature profiles for different A (>0, decelerating unsteady flow).

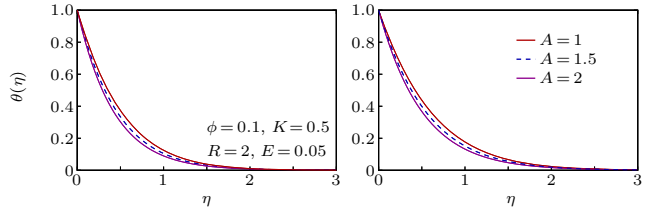

Fig. 16. Temperature profiles for different A (>0, accelerating unsteady flow).

The nanofluid temperature profiles are depicted in Figs. 17 and 18 for different values of the radiation parameter and the Eckert number, respectively. For thermal radiation, the thermal BLT is expanded and it takes place because the radiative heat transfer disturbs the temperature in a free stream for a longer distance from the flat surface. The growth of thermal BLT is meaningfully large for blade-nanoparticles and so this thermal BLT expansion due to radiation is crucial in several engineering processes, like seawater desalinization, solar thermal chemical reaction and combustor,[27] when the choice of shape of the nanoparticles is made. For growth in the Eckert number, the temperature inside nanofluid boundary layer shows an increasing trend.

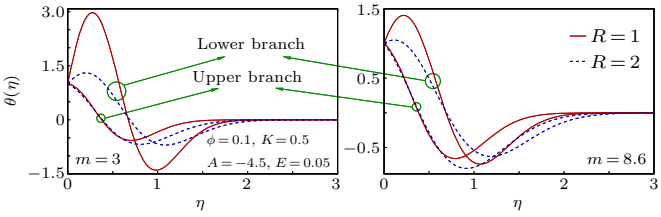

Fig. 17. Temperature profiles for different R.

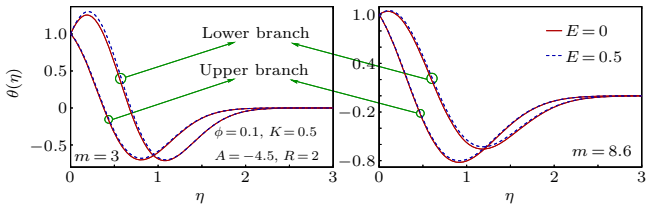

Fig. 18. Temperature profiles for different E.

5. Stability analysis of obtained solutions

Due to the existence of dual solutions for a specific range of unsteady parameter (for decelerating unsteady flow) along with a unique solution (for steady and accelerating unsteady flow), it becomes necessary to check the stability of those solutions. So, a stability analysis is performed following Weid-

man *et al.*[42] and Bakar *et al.*[43] A new dimensionless similarity variable τ is introduced and the similarity solutions are taken as

$$\psi = \sqrt{x\upsilon_f u_e} F(\eta,\tau),$$
$$T = T_\infty + (T_w - T_\infty)\Phi(\eta,\tau),$$
$$\eta = \sqrt{\frac{u_e}{x\upsilon_f}}y,$$
$$\tau = \frac{u_e t}{x}. \tag{15}$$

Using Eq. (15), Eqs. (2) and (3) with Eq. (4) reduce to

$$\frac{1}{\phi_1}\frac{\partial^3 F}{\partial\eta^3} + F\frac{\partial^2 F}{\partial\eta^2} - \left(\frac{\partial F}{\partial\eta}\right)^2 + 1 + \frac{K}{\phi_1}\left(1 - \frac{\partial F}{\partial\eta}\right)$$
$$-A\left(\frac{\partial F}{\partial\eta} + \frac{\eta}{2}\frac{\partial^2 F}{\partial\eta^2} - 1 + \tau\frac{\partial^2 F}{\partial\tau\partial\eta}\right) - \frac{\partial^2 F}{\partial\tau\partial\eta} = 0, \tag{16}$$

$$\frac{\kappa_{nf}/\kappa_f}{\phi_2}\left(1 + \frac{4}{3}R\right)\frac{\partial^2\Theta}{\partial\eta^2} + Pr\left(F\frac{\partial\Theta}{\partial\eta} - \frac{\partial\Theta}{\partial\tau}\right)$$
$$-APr\left(\frac{\eta}{2}\frac{\partial\Theta}{\partial\eta} + \tau\frac{\partial\Theta}{\partial\tau}\right) + \frac{PrE^*}{\phi_3}\left(\frac{\partial^2 F}{\partial\eta^2}\right)^2 = 0 \tag{17}$$

with

$$F(0,\tau) = 0,\ \ F'(0,\tau) = 0,\ \ \Theta(0,\tau) = 1,$$
$$F'(\eta,\tau) \to 1,\ \ \Theta(\eta,\tau) \to 0 \ \text{ as } \ \eta \to \infty. \tag{18}$$

In order to test the stability of solutions $f(\eta)$, $\theta(\eta)$ satisfying the BVP (10), (11), and (13), the following are introduced (Weidman *et al.*[42]):

$$F(\eta,\tau) = f(\eta) + e^{-\gamma\tau} f^*(\eta,\tau),$$
$$\Theta(\eta,\tau) = \theta(\eta) + e^{-\gamma\tau}\theta^*(\eta,\tau), \tag{19}$$

where $f^*(\eta,\tau)$, $\theta^*(\eta,\tau)$ are disturbances to solutions $f(\eta)$, $\theta(\eta)$ and are assumed very small in comparison with the solutions and γ is rate of disturbance. Using Eq. (19) in Eqs. (16)–(18) and linearizing we have

$$\frac{1}{\phi_1}\frac{\partial^3 f^*}{\partial\eta^3} + f\frac{\partial^2 f^*}{\partial\eta^2} + f^*\frac{d^2 f}{d\eta^2} - 2\frac{df}{d\eta}\frac{\partial f^*}{\partial\eta}$$
$$-A\left(\frac{\partial f^*}{\partial\eta} + \frac{\eta}{2}\frac{\partial^2 f^*}{\partial\eta^2} + \tau\frac{\partial^2 f^*}{\partial\tau\partial\eta} - \gamma\tau\frac{\partial f^*}{\partial\eta}\right)$$
$$-\frac{K}{\phi_1}\frac{\partial f^*}{\partial\eta} - \frac{\partial^2 f^*}{\partial\tau\partial\eta} + \gamma\frac{\partial f^*}{\partial\eta} = 0, \tag{20}$$

$$\frac{\kappa_{nf}/\kappa_f}{\phi_2}\frac{\partial^2\theta^*}{\partial\eta^2} + Pr\left(f\frac{\partial\theta^*}{\partial\eta} + f^*\frac{d\theta}{d\eta} - \frac{\partial\theta^*}{\partial\tau} + \gamma\theta^*\right)$$
$$-APr\left(\frac{\eta}{2}\frac{\partial\theta^*}{\partial\eta} + \tau\frac{\partial\theta^*}{\partial\tau} - \tau\gamma\theta^*\right)$$
$$+\frac{2PrE^*}{\phi_3}\frac{d^2 f}{d\eta^2}\frac{\partial^2 f^*}{\partial\eta^2} = 0 \tag{21}$$

subject to

$$f^*(0,\tau) = 0,\ \ \frac{\partial f^*}{\partial\eta}(0,\tau) = 0,\ \ \theta^*(0,\tau) = 0,$$
$$\frac{\partial f^*}{\partial\eta}(\infty,\tau) \to 0,\ \ \theta^*(\infty,\tau) \to 0. \tag{22}$$

Now, taking $\tau = 0$ and putting $f^*(\eta,\tau) = f_0^*(\eta)$ and $\theta^*(\eta,\tau) = \theta_0^*(\eta)$, $f_0^*(\eta)$ and $\theta_0^*(\eta)$ being the initial disturbances to solutions, Eqs. (20)–(22) become

$$\frac{1}{\phi_1}\frac{d^3 f_0^*}{d\eta^3} + f\frac{d^2 f_0^*}{d\eta^2} + f_0^*\frac{d^2 f}{d\eta^2} - 2\frac{df}{d\eta}\frac{df_0^*}{d\eta}$$
$$-A\left(\frac{df_0^*}{d\eta} + \frac{\eta}{2}\frac{d^2 f_0^*}{d\eta^2}\right) - \frac{K}{\phi_1}\frac{df_0^*}{d\eta} + \gamma\frac{df_0^*}{d\eta} = 0, \tag{23}$$

$$\frac{\kappa_{nf}/\kappa_f}{\phi_2}\frac{d^2\theta_0^*}{d\eta^2} + Pr\left(f\frac{d\theta_0^*}{d\eta} + f_0^*\frac{d\theta}{d\eta} + \gamma\theta_0^*\right)$$
$$-\frac{\eta APr}{2}\frac{d\theta_0^*}{d\eta} + \frac{2PrE^*}{\phi_3}\frac{d^2 f}{d\eta^2}\frac{d^2 f_0^*}{d\eta^2} = 0 \tag{24}$$

with

$$f_0^*(0) = 0,\ \ \frac{df_0^*}{d\eta}(0) = 0,\ \ \theta_0^*(0) = 0,$$
$$\frac{df_0^*}{d\eta}(\infty) \to 0,\ \ \theta_0^*(\infty) \to 0. \tag{25}$$

Equations (23) and (24) with Eq. (25) constitute an eigenvalue problem with γ an eigenvalue, to be determined. An infinite set of eigenvalues $\gamma_1 < \gamma_2 < \gamma_3 < \cdots$ will be obtained on solving the eigenvalue problem (23)–(25). The least eigenvalue γ_1 will regulate the stability of the solutions $f(\eta)$ and $\theta(\eta)$. If γ_1 has a positive value, then there will be an initial decay of disturbances to the solutions and in this case, the solutions will be stable. Now, if γ_1 has a negative value, then there is a clear indication of initial growth of disturbances to the solutions and hence the solutions will be unstable.

After solving the above eigenvalue problem, the smallest eigenvalues γ_1 are listed in Table 4 for upper and lower branch solutions ($A_c \le A < 0$, decelerating unsteady flow) and the unique solution ($A \ge 0$, steady and accelerating unsteady flow) for some values of A with $\varphi = 0.1$ and $K = 0.5$. The values of γ_1 for the upper branch solution and the unique solution are found to be positive, while for the lower branch solution its value is negative. So, from the aforesaid analysis, it may be resolved that the upper branch and unique solutions are stable solutions, whereas the lower branch solution is an unstable solution. The stability or instability of solutions is not able to guarantee its physical existence or non-existence in real experiments. If an experiment is performed, then there will be two possibilities for decelerating unsteady flow ($0 > A \ge A_c$). There may be a real and visible boundary layer flow or no boundary layer formulation in the flow field. It means that when a stable solution occurs, it will be real and visible and when an unstable solution arises, it will have no physical existence, i.e., due to many unavoidable disturbances during the experiment it will not be physically realizable. So, we may say that both solutions have physical meaning and relevance.

Table 4. Smallest eigenvalue, γ_1 for some values of A with $\phi = 0.1$ and $K = 0.5$.

A	γ_1
2	4.9075918
1	3.8994496
0	3.5090404
−1	3.14072230 [−2.1280794]
−2	2.7633561 [−2.1698782]
−3	2.3554984 [−1.9928801]
−4	1.8871452 [−1.6830540]
−5	1.2872198 [−1.2018309]
−5.5	0.8583381 [−0.8222378]
−5.8	0.4457369 [−0.4365984]
−5.9	0.1526771 [−0.1522516]
−5.91	0.0777469 [−0.0781784]
−5.913	0.0301721 [−0.0304514]

[ ] Values for the lower branch solution.

6. Concluding remarks

The unsteady stagnation-point flow of Cu–H_2O nanofluid on a flat surface in a porous medium is investigated taking effects of various shapes of Cu-nanoparticles. The effects of viscous dissipation and thermal radiation are taken into consideration. The governing equations of the problem are converted into self-similar coupled ODEs which constitute a BVP and it is solved by a shooting method. After a complete analysis, a summary of findings is as follows:

(i) Dual solutions exist for any value of the decelerating unsteady parameter ($A < 0$), i.e., decelerating unsteady flow and these solutions exist up to a certain critical value A_c (< 0). Whereas, for accelerating unsteady and steady flows ($A \geq 0$), the solution is unique.

(ii) Only the presence of nanoparticles does not affect the value of A_c, but when flow is considered in a porous medium then the magnitude of A_c decreases with nanoparticle volume fraction. Also, due to larger permeability parameter, the range of existence of dual solutions is longer.

(iii) The shapes of nanoparticles have no influence on the value of A_c, but it has a huge impact on surface heat transfer.

(iv) The Nusselt number, i.e., the cooling rate enhances with increasing values of shape factor m and the presence of thermal radiation. Also, for upper branch and unique solutions, the drag force and cooling rate rise with K.

(v) For the positive Eckert number, a minor reduction in the cooling rate is observed in some cases of decelerating unsteady flow and for the accelerating unsteady flow a contrasting effect is found.

(vi) For the upper branch solution, the velocity rises with K along with a reduction in BLT and the opposite nature exhibits for the lower branch. Whereas, despite an initial decay of temperature, the thermal BLT enhances with m.

(vii) For decelerating unsteady flow ($A < 0$), velocity reduces in the upper branch and it increases for accelerating unsteady flow ($A > 0$). Opposite trends are observed in temperature.

(viii) After the stability analysis, it is obtained that the upper branch and unique solutions are stable, whereas the lower branch solution is unstable.

References

[1] Choi S U S 1995 *In: D.A. Siginer and H.P. Wang, Eds., Developments and Applications of Non-Newtonian Flows, ASME, New York* **66** 99
[2] Buongiorno J 2006 *ASME J. Heat Transf.* **128** 240
[3] Tiwari R K and Das M K 2007 *Int. J. Heat Mass Transf.* **50** 2002
[4] Maxwell J C 1881 *A Treatise on Electricity and Magnetism* (2nd edn.) (Oxford: Clarendon Press) UK
[5] Hamilton R L and Crosser O K 1962 *Ind. Eng. Chem. Fundam.* **1** 187
[6] Yu W and Choi S U S 2003 *J. Nanoparticle Res.* **5** 167
[7] Jang S P and Choi S U S 2004 *Appl. Phys. Lett.* **84** 4316
[8] Beck M P, Sun T F and Teja A S 2007 *Fluid Phase Equilibr.* **260** 275
[9] Timofeeva E V, Routbort J L and Singh D 2009 *J. Appl. Phys.* **106** 014304
[10] Ellahi R, Hassan M and Zeeshan A 2015 *Int. J. Heat Mass Transf.* **81** 449
[11] Hamid M, Usman M, Zubair T, Ul Haq R and Wang W 2018 *Int. J. Heat Mass Transf.* **124** 706
[12] Akbar N S, Butt A W and Tripathi D 2017 *Res. Phys.* **7** 2477
[13] Dogonchi A S, Waqas M, Seyyedi S M, Tilehnoee M H and Ganji D D 2019 *Int. J. Heat Mass Transf.* **132** 473
[14] Dogonchi A S, Tilehnoee M H, Waqas M, Seyyedi S M, Animasaun I L and Ganji D D 2020 *Physica A* **540** 123034
[15] Hosseinzadeh K, Roghani S, Asadi A, Mogharrebi A and Ganji D D 2021 *Int. J. Numer. Methods Heat Fluid Flow* **31** 402
[16] Tlili I, Samrat S P, Sandeep N and Nabwey H A 2021 *Ain Shams Eng. J.* **12** 935
[17] Iftikhar N, Rehman A and Sadaf H 2021 *Int. Commun. Heat Mass Transf.* **120** 105012
[18] Nield D A and Kuznetsov A V 2009 *Int. J. Heat Mass Transf.* **52** 5796
[19] Kuznetsov A V and Nield D A Transp 2010 *Transp. Porous Media* **81** 409
[20] Ahmad S and Pop I 2010 *Int. Commun. Heat Mass Transf.* **37** 987
[21] Gorla R S R, Chamkha A J and Rashad A M 2011 *Nanoscale Res. Lett.* **6** 207
[22] Hatami M and Ganji D D 2013 *J. Mol. Liq.* **188** 155
[23] Xu H, Gong L, Huang S and Xu M 2015 *Int. J. Heat Mass Transf.* **83** 399
[24] Xu H and Xing Z 2017 *Int. Commun. Heat Mass Transf.* **89** 73
[25] Xu H, Xing Z and Vafai K 2019 *Int. J. Heat Fluid Flow* **77** 242
[26] Xu H, Xing Z B and Ghahremannezhad A 2019 *J. Porous Media* **22** 1553
[27] Xu H J, Xing Z B, Wang F Q and Cheng Z M 2019 *Chem. Eng. Sci.* **195** 462

[28] Mehryan S A M, Sheremet M A, Soltani M and Izadi M 2019 *J. Mol. Liq.* **277** 959
[29] Roşca A V, Roşca N C and Pop I 2021 *Int. J. Numer. Methods Heat Fluid Flow* **31** 75
[30] Oztop H F and Abu-Nada E 2008 *Int. J. Heat Fluid Flow* **29** 1326
[31] El-Aziz M A 2014 *J. Egypt. Math. Soc.* **22** 529
[32] Seddeek M A and Abdelmeguid M S 2006 *Phys. Lett. A* **348** 172
[33] Seth G S, Singha A K, Mandal M S, Banerjee A and Bhattacharyya K 2017 *Int. J. Mech. Sci.* **134** 98
[34] Mukhopadhyay S and Mandal I C 2014 *Chin. Phys. B* **23** 044702
[35] Bhattacharyya K and Pop I 2014 *Chin. Phys. B* **23** 024701
[36] Mukhopadhyay S 2014 *Chin. Phys. B* **23** 014702
[37] Bhattacharyya K, Hayat T and Alsaedi A 2014 *Chin. Phys. B* **23** 124701
[38] Bhattacharyya K 2011 *Chin. Phys. Lett.* **28** 084702
[39] Pandey A K, Rajput S, Bhattacharyya K and Sibanda P 2021 *Pramana-J. Phys.* **95** 5
[40] Bachok N, Ishak A and Pop I 2012 *Int. J. Heat Mass Transf.* **55** 6499
[41] Salem A M, Ismai G and Fathy R 2015 *Eur. Phys. J. Plus* **130** 113
[42] Weidman P D, Kubitschek D G and Davis A M J 2006 *Int. J. Eng. Sci.* **44** 730
[43] Bakar A, Arifin N M, Ali M F, Bachok N, Nazar R and Pop I 2018 *Appl. Sci.* **8** 483